

The effect of rapeseed oil biodiesel fuel on combustion, performance, and the emission formation process within a heavy-duty DI diesel engine



Luka Lešnik*, Ignacijo Biluš

University of Maribor, Faculty of Mechanical Engineering, Smetanova 17, SI-2000 Maribor, Slovenia

ARTICLE INFO

Article history:

Received 11 September 2015

Accepted 1 December 2015

Available online 17 December 2015

Keywords:

Biofuels

Emission reduction

Combustion process

Sub-model for parameter determining

Emission formation

ABSTRACT

This study presents the influence of biodiesel fuel and blends with mineral diesel fuel on diesel engine performance, the combustion process, and the formation of emissions. The study was conducted numerically and experimentally. The aim of the study was to test the possibility of replacing mineral diesel fuel with biodiesel fuel made from rapeseed oil. Pure biodiesel fuel and three blends of biodiesel fuel with mineral diesel fuel were tested experimentally for that purpose on a heavy-duty bus diesel engine. The engine's performance, in-cylinder pressure, fuel consumption, and the amount of produced NO_x and CO emissions were monitored during experimental measurements, which were repeated numerically using the AVL BOOST simulation program. New empirical sub-models are proposed for determining a combustion model and emission models parameters. The proposed sub-models allow the determination of necessary combustion and emission model parameters regarding the properties of the tested fuel and the engine speed. When increasing the percentage of biodiesel fuel within the fuel blends, the reduction in engine torque and brake mean effective pressures are obtained for most of the test regimes. The reduction is caused due to the lower calorific value of the biodiesel fuel. Higher oxygen content in biodiesel fuel contributes to a better oxidation process within the combustion chamber when running on pure biodiesel or its blends. Better oxidation further results in a reduction of the formatted carbon and nitrogen oxides. The reduction of carbon emission is also attributed to the biodiesel fuel's lower carbon content. It can be concluded from the obtained results that neat biodiesel fuel and its blends with mineral diesel fuel can be used in heavy-duty diesel engines with mechanically controlled injection systems as replacements for mineral diesel fuel. The agreement between numerical and experimental results confirms the usability of the proposed sub-model. The sub-models decrease time needed to preform numerical simulations with a reasonable amount of confidence without experimental results.

© 2015 Elsevier Ltd. All rights reserved.

1. Introduction

Interest in the usage of biofuels is increasing yearly due to their lower environmental impacts compared to fossil fuels, their contributions to reducing greenhouse gas emissions, and their potential for use as an alternative fuel. The usage of biofuel in Europe is also promoted by the rising prices of neat diesel fuel, European Union directives, and the Kyoto protocol directives [1–3]. Within the European Union the transport sector contributes up to 19.7% of total emissions released [4], which indicates huge potential for future reductions in emissions, where biofuels can make a significant contribution.

Compression ignition diesel engines are the most commonly used engines in modern light- and heavy-duty vehicles due to their

high efficiency levels. The biofuels' physical and chemical properties highly depend on the raw materials used for biofuel production and have a significant influence on combustion and emission formation processes [1,5,6]. First-generation biofuels like bioethanol and biodiesel have the largest scope among currently used biofuels because they can be used in existing engines with only slight modifications [7,8].

Several experimental tests should usually be conducted before introducing new types of biofuel for commercial usage within internal combustion engines. Diesel engine combustion, performance, and emission formation can be quickly and precisely described numerically using phenomenological combustion models [9]. These are based on the physical and chemical descriptions of processes taking place within the combustion chamber and are suitable for performing several parametric studies. Since the injection process in diesel engines can be predicted in advance [10] phenomenological combustion models can be used for numerical testing when introducing a new type of biofuel.

* Corresponding author.

E-mail address: llesnik@gmail.com (L. Lešnik).

Nomenclature

Q	heat (J)
I	integral
α	angle ($^{\circ}$ CA)
τ	duration ($^{\circ}$ CA/ms)
C	constant/parameter
k	density of turbulent kinetic energy
E	energy (J)
λ	air excess ratio
CV	calorific value (MJ/kg)
CN	cetane number
X	oxygen content

Subscripts

c	cylinder
MCC	mixing controlled combustion
PMC	premixed combustion
IDCF	ignition delay calibration factor
UB	unburned zone
ref	reference
id	ignition delay
SOI	start of injection
fv	vaporized fuel
kin	kinetic
f	fuel injected
$diff$	diffusion

$stoich$	stoichiometric
f	fuel
inj	injection
$turb$	turbulence
$diss$	dissipation
epx	experimentally obtained
ns	numerically obtained

Abbreviation

D2	diesel fuel
B100	pure biodiesel fuel
B25	blend of 25% biodiesel fuel with D2
B50	blend of 50% biodiesel fuel with D2
B75	blend of 75% biodiesel fuel with D2
CO	carbon monoxide
CO ₂	carbon dioxide
O ₂	oxygen
NO _x	nitrogen oxides
HC	hydro carbon
MCC	mixing controlled combustion
CA	crank angle
BTDC	before top dead center
L–M	Levenberg–Marquardt
BSFC	brake specific fuel consumption

Biodiesel produced from rapeseed oil is the more commonly used biodiesel fuel in European countries [10]. Kegl [11] and Hribernik [12] performed several experimental tests using rapeseed oil biodiesel. They observed that the higher density and kinematic viscosity of rapeseed oil biodiesel influences the earlier starting of the injection process, which increases the engine's hourly fuel consumption. The oxygen content of this biodiesel fuel reduces the amount of produced CO, HC, and soot emissions. Due to a higher cetane number and oxygen content of the biodiesel fuel, the ignition delay interval and the amount of fuel burned during the pre-mix part of combustion are reduced. The results of biodiesel's influence on diesel engine operation and emission formation depend on the test-engine type and the biodiesel's properties. This thus sometimes causes the obtained results to be contradictory, such as when comparing the results from [13] to the results of Kegl [11] and Hribernik [12]. Increases in smoke, CO and HC emissions were obtained during the study conducted by Qi et al. [13], where they tested how the use of rapeseed oil biodiesel fuel blended with conventional diesel fuel influences the combustion and emission characteristics in two-cylinder agricultural diesel engines. Waste cooking oils are also a very commonly used raw material for biodiesel production. Can [14] used two different waste cooking oils provided from a cooking factory and fast food restaurant for the production of biodiesel fuel. Two blends with 5% and 10% of biodiesel fuel were blended with diesel fuel and experimentally tested in a single-cylinder, four-stroke DI diesel engine. An earlier start of injection and combustion was also obtained when adding cooking oil biodiesel fuel to the diesel fuel. An increase in brake specific fuel consumption and NO_x emissions was obtained when using biodiesel–diesel fuel blends. The addition of biodiesel fuel causes a decrease in CO emissions at full engine load. The decrease in CO emissions was also obtained by Arbab et al. [15] when using blends of palm and coconut biodiesel fuel and by How et al. [16] when using coconut biodiesel fuel in diesel engines. The usage of palm and coconut biodiesel fuel also increases brake specific fuel consumption under most test regimes in [15]. Awad et al. [17]

achieved a drastic reduction in hydrocarbon emission formation. They used animal-fat residues collected from fat-traps to produce biodiesel fuel using a two-step acid catalyzed process. Slighter reductions of NO_x and PM emissions were obtained when burning animal fat residue biodiesel (AFRBD) while no significant changes in CO emissions were noticed. Usage of AFRBD led to a reduction of the ignition delay interval, which further influenced higher peaks of in-cylinder pressure and higher exhaust gas temperatures. Ethanol is considered a promising fuel oxygenizer that can contribute to particulate matter (PM) emission reduction [18]. Adding ethanol to diesel–biodiesel blends can help decrease the higher blend kinematic viscosity and density caused by biodiesel fuel. Tse et al. [19] concluded that diesel–biodiesel–ethanol fuel blends reduce the lower brake specific particulate mass and brake specific particulate number of concentrations compared to diesel fuel. Zhou et al. [20] tested how the addition of methanol to biodiesel fuel influences performance, combustion, and emission characteristics in reactivity controlled compression ignition (RCCI) engine. They concluded that methanol could reduce CO and soot emissions at high engine loads, where higher peak in-cylinder pressures and larger premixed ratios were obtained. The influence of methanol on biodiesel's oxidation and emission formation in a diesel engine was also tested in [21], where the indicated CO and soot emissions were decreased by increasing the addition of methanol.

In the presented paper the influences of rapeseed oil biodiesel fuel and its blends with diesel fuel on engine performance, combustion, and emission formation processes were studied numerically and experimentally. The study was carried out on three engine operation regimes under full engine loads. Numerical and experimental testing was performed on optimal static fuel delivery angles for each type of fuel, as determined in a previous paper [16]. The optimal static fuel delivery angles for used fuels and test engine provide for the optimal agreement between all engine characteristics like engine torque, specific fuel consumption, exhaust gas temperature, etc. on several engine loads and speeds. The test engine was placed on an engine test bed and equipped with a mea-

suring system. Numerical simulations were performed using the AVL BOOST simulation program and a mixing controlled combustion model. A sub-model for determining the combustion model's parameter, as proposed in a previous paper [23], was improved (optimized) in order to obtain more accurate parameter values and final numerical results. Further a new sub-model for determining an emission model's parameter values based on the used fuel properties and engine speed is proposed in the presented paper. The newly proposed sub-model for determining the emission model's parameters and the optimized sub-model for determining the combustion model's parameters introduce novelties within engine simulations. They were further used for calculating the needed combustion and emission model parameters for all five tested fuels. The determined values of model parameters allowed to numerical repeat experimental measurements and to obtain the in-cylinder emission formation results, which are hard to obtain experimentally. Good agreement between the numerical and experimental results validates the newly proposed and optimized sub-models.

2. Test fuels

Neat mineral diesel fuel (D2) containing no additives and neat biodiesel fuel (B100) produced from rapeseed oil, which is the most commonly used biodiesel fuel in Slovenia, were used in the present study. Their blends of diesel and biodiesel fuels were made from pure diesel and biodiesel fuels. The blends were made in three different volume ratios of biodiesel blended with diesel fuel. The volume ratios of biodiesel fuel were 25% for B25, 50% for B50, and 75% for the B75 fuel blend. The selected volume ratios of biodiesel consider the full interval (0–100%) of biodiesel–diesel fuel blends. Some of the fuel properties presented in Table 1 were provided by the supplier, while others measured in [5,7,10,11]. The test methods used for measuring fuel properties corresponded to

European or other test standards are also presented in the aforementioned references. The fuels' sound velocities were measured at different pressures up to 700 bar and are presented in Fig. 1. The presented properties of the fuels were implemented within the numerical program in order to include the real properties of biodiesel fuel and its blends with diesel fuel in numerical simulation.

3. Experimental set-up

All the experimental measurements presented in this study were performed on a 6 cylinder, naturally aspirated, water-cooled, MAN D2566 MUM, four-stroke, heavy-duty diesel engine. This engine was equipped with a Bosch PES6A95D410LS2542 high-pressure in-line injection pump, which delivered fuel to six Bosch DLLA 5S834 injectors with one injection hole. The engine has an M-combustion system and was placed on an engine test-bed. The engine test-bed was equipped with a Zöllner B – 305 AC eddy current engine dynamometer, which is designed for operating within a range of 0–6500 rotations per minute. It can measure engine torque up to 2000 N m with an accuracy of $\pm 0.2\%$. Pressure in the engine's combustion chamber was measured using a Kistler 6001 piezoelectric pressure transducer mounted in the first engine cylinder. This pressure transducer can measure dynamic pressure up to 250 bar and has an accuracy of $\pm 0.8\%$. The AVL Fuel Balance 730 dynamic measuring system was used for measuring engine fuel consumption. The fuel consumption measuring was based on the differences of fuel mass in the measuring vessel at specific time intervals. The fuel consumption meter can measure fuel consumption up to 150 kg/h and has an accuracy of $\pm 0.12\%$ of measuring range. A RMG Messtechnik air-flow meter was used for measuring the engine's hourly air consumption. A chemiluminescence analyzer from Thermoenvironmental Instruments and a MAIHAK UNOR 610 analyzer were used for measuring NO_x and CO emission

Table 1
Tested fuels' properties [5,7,10,11].

Fuel	Test method	D2	B25	B50	B75	B100
Density at 15 °C (kg/m^3)	EN ISO 12185	838.8	850.3	861.8	873.3	884.8
Kin. viscosity at 30 °C (mm^2/s)	EN ISO 3104	3.34	3.9	4.4	4.9	5.5
Surface tension at 30 °C (N/m)	(supplier)	0.02655	0.02613	0.02675	0.02738	0.028
Caloric value (MJ/kg)	ASTN D 4868	42.8	41.5	40.5	39.4	38.2
Cetane number	EN ISO 5165	45	46.5	48	49.5	51
Stoichiometric air–fuel ratio	–	14.7	14.3	13.8	13.4	13
Flash point (°C)	EN ISO 2719	66	84.1	102.5	120.4	138.5
Carbon (C) mass fraction	ASTM D 5291	0.86	0.84	0.82	0.79	0.78
Hydrogen (H) mass fraction	ASTM D 5291	0.134	0.131	0.128	0.12425	0.121
Sulfur (S) mass fraction	ISO 20884	0.003	0.0025	0.002	0.0015	0.001
Oxygen (O) mass fraction	(supplier)	–	0.026	0.052	0.078	0.10
Water content (mg/kg)	EN ISO 12937	50	75	100	125	150

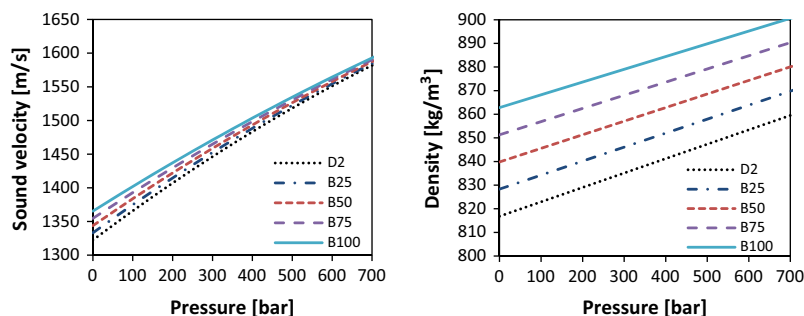


Fig. 1. Tested fuels' properties.

concentrations within the exhaust gases. A NO_x analyzer can measure concentrations within the range of 0–10,000 ppm with an accuracy of ±1% of measuring range. The amount of NO_x molecules in exhaust gases is measured based on the amount of detected light emissions that appear as a bi-product of the chemiluminescent reaction of NO + O₃ in NO₂ + O₂. The concentration of CO emissions in exhaust gases is measured based on the amount of infrared light absorption through the exhaust gas sample. The accuracy of the MAIHAK CO analyzer is 1%, with a measuring range from 0 to 1000 ppm. Omega type J thermocouples were used for measuring the temperatures within different engine parts. They can measure temperatures between –40 and 750 °C with accuracies of ±1.5 °C. The computer application made in the LabVIEW program and the data acquisition system were used for storing measured values. All exhaust gas samples were adjusted and prepared according to used measuring device standards.

Engine tests (operating) regimes, engine speed, and throttle position (load) were the same for all fuels and correspond to three points (2, 8, and 10) of the 13 mode ESC test. The engine was tested on three different test regimes using different engine speeds (1360, 1700, and 2000 rpm). All the tests were made on full throttle positions where the maximal quantity of each tested fuel was delivered for all engine speeds. The test engine obtained maximal engine load for each tested fuel on all three test regimes. Optimal static fuel delivery angles, determined in previous study [16], were used for each fuel on all engine speeds.

The measurements were conducted within five sections; in each section the different fuel was used on its optimal static fuel delivery angle [11]. Using the measured in-cylinder pressures traces and the one-zone zero dimensional combustion model described in [24] heat release curves were predicted. Engine specifications and static fuel delivery angles for each fuel and are presented in Table 2.

Experimental and numerical results of biodiesel's influence on injection systems' operating conditions are not presented in this paper. They were studied and detailed presented in previous work [30].

4. Simulation model

The AVL BOOST simulation program was used for numerical testing of test engine. The mixing-controlled combustion model (MCC) developed by Chmela and Orthaber was used for calculating the test engine's performance and heat release. The concentration of formatted CO emissions was calculated using an Onorati CO formation model, while NO_x emissions were calculated using the Patas and Häfner NO_x emission model. Some of the important combustion model and emissions model equations are presented within the following sections. For detailed descriptions of the models refer to [22,25].

Table 2
Test engine specifications.

Engine type	MAN D2566 MUM four-stroke
Gas exchange	Naturally aspirated
Number of cylinders	6
Bore (mm)	125
Stroke (mm)	155
Total displacement (ccm)	11413
Compression ratio	17.5
Fueling	Direct injection
Fuel pump	BOSCH PES6A95D410LS2542
Injection nozzle	BOSCH DLLA 5S834
Start of injection process (° BTDC)	23-D2; 22-B25; 21-B50; 20-B75; 19-B100

4.1. Combustion model

The MCC combustion model developed by Chmela and Orthaber was used for calculating the test engine's performance and conditions within its engine combustion chamber. The model divides combustion into premixed (kinetic) and mixing-controlled (diffusion) combustion stages. The total released heat during combustion Q_c is the sum of the released heat during the premixing stage Q_{PMC} and the released heat during the mixing-controlled combustion stage Q_{MCC} :

$$Q_c = Q_{PMC} + Q_{MCC} \quad (1)$$

Premixed combustion occurs when the ignition delay interval ends and the fuel vapors mixed with air ignite. The duration of the ignition delay τ_{id} and the crankshaft angle α_{id} at which the ignition delay ends and combustion begins were calculated using an ignition delay model developed by Andree and Pachernegg [25,26]. As soon as the ignition delay integral I_{id} reached the value ≥ 1 , the duration of ignition delay was calculated as:

$$\frac{dI_{id}}{d\alpha} = \frac{1}{C_{IDCF}} \cdot \frac{T_{UB} - T_{ref}}{Q_{ref}} \quad (2)$$

$$\tau_{id} = \alpha_{id} - \alpha_{SOI} \quad (3)$$

where C_{IDCF} represents the ignition delay calibration factor, T_{UB} the non-burned zone temperature, T_{ref} the reference temperature and Q_{ref} the reference activation energy, and α_{SOI} is the start of the injection process which is defined by the injection rate curve.

The combustion process within the premixed part of combustion is very fast because the fuels' vapors are already mixed with air. The rate of released heat in the premixed part of the combustion was calculated using the well-known Vibe function, where the shape parameter was set at 2 and the Vibe parameter at 6.9 [22,25]. The amount of combusted fuel mass injected during ignition delay must be set by the user using a premixed combustion model parameter.

The fuel injected after the start of combustion is burned during the mixing-controlled stage of combustion. The total amount of released heat at this stage of combustion was a function of the vaporized fuel mass m_{fv} available for combustion and the turbulent kinetic energy density k within the cylinder. The rate of heat released during the mixing-controlled part of combustion is written as:

$$\frac{dQ_{MCC}}{d\alpha} = C_{comb} \cdot \left(m_{fv} - \frac{Q_{MCC}}{LCV} \right) \cdot w_{O2,a} \cdot C_{Rate} \cdot \frac{\sqrt{k}}{\sqrt[3]{V_c}} \quad (4)$$

where C_{comb} represents the combustion constant, $w_{O2,a}$ the amount of oxygen available for combustion, C_{Rate} the mixing rate constant, and V_c the cylinder volume.

The combustion constant influences the fuel combustion speed, Eq. (4). The local density of the turbulent kinetic energy is a function of the mixing rate constant and cylinder volume. It can be calculated using the following equations:

$$k = \frac{E_{kin}}{m_{f,inj} \cdot (1 + \lambda_{diff} \cdot m_{stoich})} \quad (5)$$

$$\frac{dE_{kin}}{dt} = 0.5 \cdot C_{turb} \cdot \dot{m}_f (v_{inj})^2 - C_{diss} \cdot E_{kin}^{1.5} \quad (6)$$

where E_{kin} represents the fuel jet kinetic energy, $m_{f,inj}$ the injected fuel mass, λ_{diff} the air excess ratio, m_{stoich} the stoichiometric mass of fresh charge, C_{turb} the turbulent energy production constant, \dot{m}_f the fuel mass flow, v_{inj} the fuel injection velocity, and C_{diss} the dissipation constant.

With usage of the turbulent energy production and dissipation constants, the influence of the fuel spray jet kinetic energy and dissipation process on the fuel combustion process is controlled. The combustion model is described in more detailed in [25].

4.2. Emission formation models

The used emission model for the computation of NO_x formation is based on the Pattas and Häfner NO_x formation model [27]. The rate of NO_x formation was computed using Eq. (7):

$$r_{\text{NO}} = C_{KM} \cdot 2 \cdot (1 - \alpha_{\text{NO}}^2) \cdot \frac{r_{1,\text{NO}}}{1 + \alpha_{\text{NO}} R_2} \cdot \frac{r_{4,\text{NO}}}{1 + R_4} \quad (7)$$

where C_{KM} represents the NO_x formation kinetic multiplier, α_{NO} the ratio between the actual (calculated) $c_{\text{NO,act}}$ and equilibrium $c_{\text{NO,equ}}$ NO molar mass, and $r_{i,\text{NO}}$ the reaction rates of the Zeldovich mechanism.

The NO molar mass ratio could be calculated using Eq. (8):

$$\alpha_{\text{NO}} = \frac{c_{\text{NO,act}}}{C_{PM} \cdot c_{\text{NO,equ}}} \quad (8)$$

The CO emission formation model used was based on the Onorati CO formation model [28], which computed the final rates of the CO products as

$$r_{\text{CO}} = C_{\text{cons}} \cdot (r_{1,\text{CO}} + r_{2,\text{CO}}) \cdot (1 + \alpha_{\text{CO}}) \quad (9)$$

where C_{cons} represents the CO formation kinetic multiplier, $r_{i,\text{CO}}$ the reaction rates and α_{CO} ratio between the actual (calculated) $c_{\text{CO,act}}$ and equilibrium $c_{\text{CO,equ}}$ CO molar masses, and is calculated using Eq. (10):

$$\alpha_{\text{CO}} = \frac{c_{\text{CO,act}}}{c_{\text{CO,equ}}} \quad (10)$$

The equilibrium NO and CO molar masses of each tested fuel were automatically determined from the program's data base. The program determines the equilibrium molar masses based on fuel properties, air/fuel ratio, in-cylinder pressure and temperature. Emission models are described in more detail in [25].

5. Sub-models' derivations

Section 4 indicated the high influence of the combustion and emission model parameter on the combustion and emission formation process. The combustion and emission model parameters are usually determined based on user experience. Their final values are further tuned by comparing the experimental and numerical results, for which several simulation test runs are needed. This process is very time-consuming and needs to be repeated for each type of fuel, and tested on all test regimes. It is therefore inappropriate for larger numbers of simulations and it also does not allow us to run numerical simulations without the results of experimental measurements.

5.1. Sub-model for determination of the combustion model parameters

An empirical sub-model for the determination of the combustion model parameters was proposed in the previous work [23]. A selected combustion model parameters (C_{IDCF} , C_{comb} , and C_{PMC}) determination process was presented as an inverse problem that was solved using the Levenberg–Marquardt (L–M) optimization method. The selected combustion model's parameters presented design variables during the optimization process. Equations of the empirical sub-model for determining combustion model parameters were selected based on the determined values of the selected combustion model parameters for pure diesel and pure biodiesel fuel [23].

In the presented study the proposed sub-model from previous work has been improved in order to obtain more accurate values of model parameters and better agreement between numerical and experimental results. In previous work [23] the proposed sub-model equation forms (Eqs. (11)–(13)) were optimized for this purpose.

$$C_{\text{IDCF},ij} = \mathbf{x}_1 \cdot e^{n_j} \cdot \text{CN}_i + \mathbf{x}_2 \cdot n_j \cdot \text{CN}_i + \mathbf{x}_3 \cdot n_j^2 + \mathbf{x}_4 \cdot n_j + \mathbf{x}_5 \cdot \text{CN}_i + \mathbf{x}_6 \quad (11)$$

$$C_{\text{comb},ij} = \mathbf{x}_7 \cdot e^{n_j} \cdot \text{CV}_i + \mathbf{x}_8 \cdot n_j \cdot \text{CV}_i + \mathbf{x}_9 \cdot n_j^2 + \mathbf{x}_{10} \cdot n_j + \mathbf{x}_{11} \cdot \text{CV}_i + X_i + \mathbf{x}_{12} \quad (12)$$

$$C_{\text{PMC},ij} = \mathbf{x}_{13} \cdot n_j \cdot \text{CN}_i + \mathbf{x}_{14} \cdot n_j^2 + \mathbf{x}_{15} \cdot n_j + \mathbf{x}_{16} \cdot \text{CN}_i + \mathbf{x}_{17} \quad (13)$$

In the presented equations n_j represents the engine speed divided by 1000 at a specific engine operating regime j , the CV_i calorific value, CN_i cetane number of fuel i , and X_i fuel oxygen content.

Optimization of the sub-model for determining the combustion model's parameters was presented as an inverse problem that was solved using the L–M optimization method. The selection of optimization method is described in detail in [29].

Optimization was then performed for diesel and for biodiesel fuel on all three test regimes simultaneously, where the coefficients $\mathbf{x}_1 - \mathbf{x}_{17}$ of Eqs. (11)–(13) represent the design variable during the optimization process. The experimentally measured in-cylinder pressure trace was used as a fitting parameter within the objective function for the optimization process. Performing optimization for two fuels simultaneously on all three test regimes determines the values of the combustion model's parameters more accurately than determined in the previous work. The following forms of new (optimized) sub-models equations were determined using the optimization process:

$$C_{\text{IDCF},ij} = -0.00634 \cdot e^{n_j} \cdot \text{CN}_i + 0.0385 \cdot n_j \cdot \text{CN}_i + 0.861 \cdot n_j^2 - 3.155 \cdot n_j - 0.0318 \cdot \text{CN}_i + 3.149 \quad (14)$$

$$C_{\text{comb},ij} = -0.713 \cdot e^{n_j} \cdot \text{CV}_i + 2.750 \cdot n_j \cdot \text{CV}_i + 156.834 \cdot n_j^2 - 452.724 \cdot n_j - 0.965 \cdot \text{CV}_i + X_i + 326.519 \quad (15)$$

$$C_{\text{PMC},ij} = 0.00985 \cdot n_j \cdot \text{CN}_i - 0.864 \cdot n_j^2 + 2.0236 \cdot n_j - 0.0255 \cdot \text{CN}_i - 0.202 \quad (16)$$

The presented equations of sub-models for determining combustion model parameters were further used for calculating the combustion model parameters' values for all fuels tested.

5.2. A sub-model for determining the emission model's parameters

Derivation of the sub-model for determining the emission models' parameters was also presented as an inverse problem that was solved using the L–M optimization method. The objective function for optimization was defined for minimizing the difference between the simulation results and the experimentally-obtained results of the formatted NO_x and CO emissions.

The values of the emission model's parameters for D2, B100, and B50 fuels were determined using the L–M optimization method. Each emission model contained only one model parameter, which was used as its design variable during the optimization process. Their correct values depend on the used fuel properties and engine speed and they must be determined accurately in order to numerically simulate the real influences of tested fuels on the emission formation process. From the determined values of the emission model's parameters, the forms of sub-model equations

for determining the emission model's parameters were selected using a program made in Mathematica. The accuracies of the equations' forms were tested using the coefficient of determination R^2 and were greater than 0.97 for both selected equations, thus providing good levels of accuracy for the selected equations of the proposed sub-model.

$$C_{KM_{ij}} = \mathbf{u}_1 \cdot e^{C_{IDCF_i}} \cdot n_j + \mathbf{u}_2 \cdot e^{n_j} \cdot C_{IDCF_i} + \mathbf{u}_3 \cdot C_{IDCF_i}^4 + \mathbf{u}_4 \cdot n_j^4 + \mathbf{u}_5 \cdot C_{IDCF_i} \cdot n_j + \mathbf{u}_6 \cdot C_{IDCF_i} + \mathbf{u}_7 \cdot n_j - X_i + \mathbf{u}_8 \quad (17)$$

$$C_{Cons_{ij}} = \mathbf{u}_9 \cdot (C_i - n_j)^4 + \mathbf{u}_{10} \cdot e^{n_j} \cdot C_i^4 + \mathbf{u}_{11} \cdot e^{C_i} + \mathbf{u}_{12} \cdot C_i^3 + \mathbf{u}_{13} \cdot n^3 + \mathbf{u}_{14} \cdot C_i \cdot n_j + \mathbf{u}_{15} \cdot C_i + \mathbf{u}_{16} \cdot n_j - X_i + \mathbf{u}_{17} \quad (18)$$

The selected forms of the equation present only one of its possible forms. The amount of produced NO_x emissions highly depends on the start of the ignition, which influences the rise of temperature and pressure within the combustion chamber. Considering this dependence, the NO_x emission model parameter C_{KM} was expressed using the ignition delay calibration factor C_{IDCF} , engine speed n_j and fuel oxygen content X_i . The CO emission model parameter was expressed using fuel carbon content C_i , engine speed n_j and fuel oxygen content X_i , which all influenced the total amount of CO emissions formed.

Determination of the final forms of the sub-model equation was again presented as an inverse problem that was solved using the L–M optimization method. The final forms of the sub-model equations were determined using the optimization process, where coefficients $\mathbf{u}_1 - \mathbf{u}_{17}$ from Eqs. (17) and (18) presented the design variables. Simultaneous optimizations for three fuels on all test regimes precisely determined the values of emission model parameters.

The final selected equation forms of the sub-model for determining the emission model's parameter were determined using the optimization method, and are:

$$C_{KM_{ij}} = 176.9991 \cdot e^{C_{IDCF_i}} \cdot n_j + 27.5126 \cdot e^{n_j} \cdot C_{IDCF_i} - 290.1173 \cdot C_{IDCF_i}^4 - 0.9761 \cdot n_j^4 - 366.0803 \cdot C_{IDCF_i} \cdot n_j + 96.0399 \cdot C_{IDCF_i} - 154.2509 \cdot n_j - X_i - 21.0714 \quad (19)$$

$$C_{Cons_{ij}} = 1.6448 \cdot (C_i - n_j)^4 + 0.4703 \cdot e^{n_j} \cdot C_i^4 - 82736.836 \cdot e^{C_i} + 38213.5855 \cdot C_i^3 - 1.4288 \cdot n^3 - 3.5506 \cdot C_i \cdot n_j + 110752.54 \cdot C_i + 9.929 \cdot n_j - X_i + 75960.4979 \quad (20)$$

This newly proposed sub-model for determining an emission model's parameters allows us to calculate an emission model's parameter value based on used fuel properties. It was used for calculating the emission models' parameter values for all five tested fuels on all tested regimes.

6. Results

The influences of rapeseed oil biodiesel fuels and their blends with mineral diesel fuel on engine performance, emission formation, and the combustion process were tested experimentally and numerically. The testing was performed on a 6 cylinder, heavy-duty, DI diesel engine equipped with a mechanical injection system. Numerical simulations were made using the AVL BOOST simulation program, mixing-controlled combustion models, Pattas and Häfner NO_x , and Onorati CO formation models. The combustion and emission models parameters were calculated using the proposed sub-models. The testing was performed at three different engine speeds at full engine loads.

Fig. 2 shows the numerically and experimentally obtained results of engine rated torque for all three test regimes.

The results presented in Fig. 2 indicate that the highest experimentally obtained engine torque was observed when using B25 fuel blend on all test regimes. Numerically obtained results indicate the same trend as the experimentally obtained results, except at 2000 rpm where the highest engine torque was obtained using B75 fuel blend. The lowest engine rated torque was obtained numerically and experimentally when using B75 fuel blend at 1360 and 1700 rpm and when using pure biodiesel fuel at 2000 rpm.

The lower caloric value of biodiesel fuel and its blends influence the reduction of engine-rated torque on some test regimes compared to diesel fuel. Higher biodiesel density influences on the greater mass of injected fuel in used engine and injection system. This to some extent compensates for the reduction of biodiesel fuel calorific value and, as a result, in some test regimes the reduction of engine-rated torque was not obtained when using some of the fuel blends.

The presented results of engine torque show good agreement between the numerical and experimental results. The numerical results of engine torque are lower than the experimental results, except for the results for the B50 fuel blend, where the numerical results are higher than the experimental ones. The maximal difference between the numerical and experimental results of engine rated torque is 5%.

Fig. 3 shows the numerical and experimental results of brake mean effective pressure (BMEP).

Increasing engine speed decreases the experimentally obtained brake mean effective pressure, Fig. 3. The numerically obtained results for brake mean effective pressure show an increase in BMEP, when the engine speed was increased from 1360 rpm to 1700 rpm, and a decrease in BMEP, when the engine speed was increased to 2000 rpm. The lowest numerically and experimentally obtained values of BMEP for all fuels on all operating regimes were obtained at 2000 rpm. The decrease in obtained BMEP is also caused by lower engine rated torque. Lower caloric value of biodiesel fuel also contributes to a reduction of BMEP on some test regimes compared to diesel fuel.

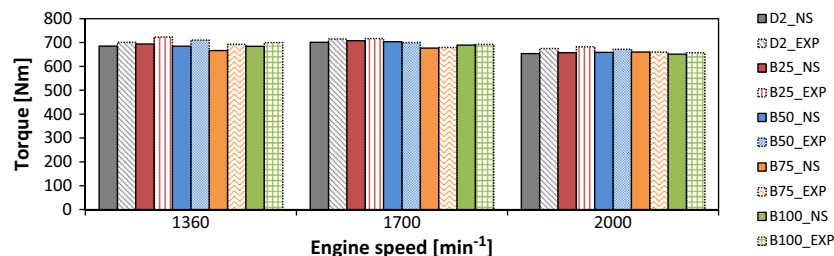


Fig. 2. Numerical and experimental rated engine torque.

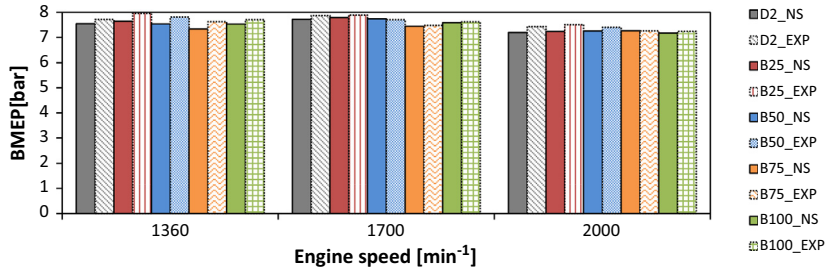


Fig. 3. Numerical and experimental rated engine BMEP.

The maximal difference between the numerical and experimental results of BMEP is 4%.

The difference in biodiesel fuel properties influences the advance start of the injection process in the used mechanical controlled injection system [22]. This further influence on greater amount of injected biodiesel fuel and its blends. The greater amount of injected fuel increases hourly fuel consumption and influences the brake-specific fuel consumption (BSFC), which is increased when using pure biodiesel fuel or fuel blends, Fig. 4.

Increasing the percentage of biodiesel fuel has an influence on the brake-specific fuel consumption increase. The experimental results show an increase in BSFC when the engine speed is

increased, while the numerical results show a slight decrease in BSFC when increasing the engine speed from 1360 rpm to 1700 rpm, and an increase in BSFC when the engine speed is increased from 1700 to 2000 rpm. Maximal values of BSFC for all tested fuels were obtained at 2000 rpm. The decrease in the numerical results of BSFC is a result of different trends regarding the numerical and experimental results of engine rated torque.

The maximal difference between the numerical and experimental results of BSFC is 6%.

Fuel chemical composition and the engine operating regime influence the amount of formatted NO_x and CO emissions, as presented in Figs. 5 and 6. The amount of emissions formed is also

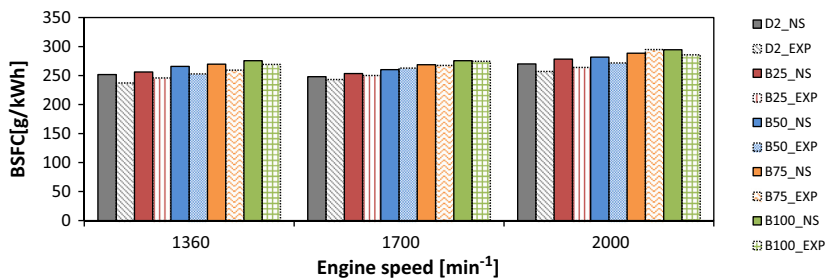


Fig. 4. Numerical and experimental rated engine BSFC.

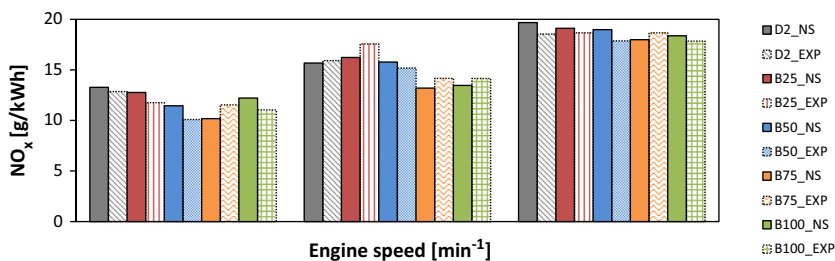


Fig. 5. Numerical and experimental results of specific NO_x emissions.

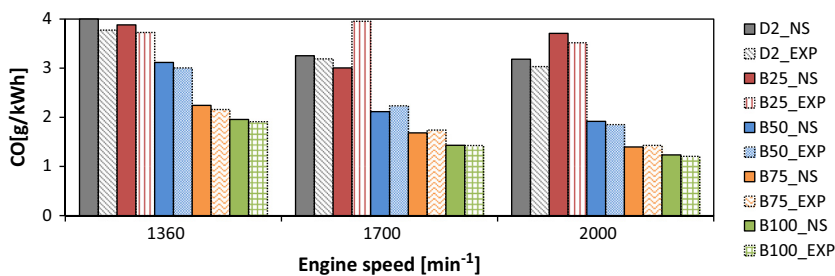


Fig. 6. Numerical and experimental results of specific CO emissions.

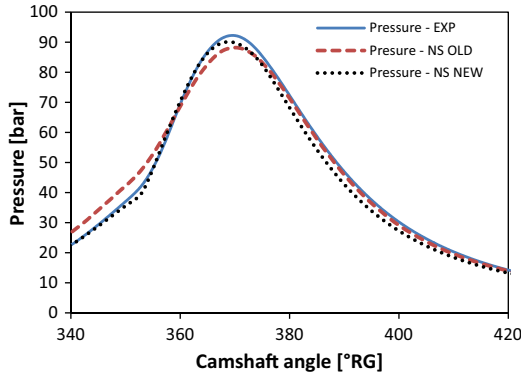


Fig. 7. Comparison of new and old sub-models.

influenced by the start of injection, which depends on the tested fuels' properties and static fuel delivery angles.

The results of specific emissions indicate that when increasing engine speed the amount of formatted NO_x emissions is increased and the amount of formatted CO emissions is decreased. The highest amount of specific NO_x emission was numerically and experimentally obtained at the maximum engine test speed for all fuels, where we also obtained maximal in-cylinder pressure and temperature. The highest amount of CO emissions formatted was obtained at the lowest engine speed except for the experimental results of B25 fuel blend, where the maximal amount of CO emissions was formed at 1700 rpm. The lowest concentration of NO_x emission was obtained numerically when using the B75 fuel blend at all engine speeds and experimentally when using the B50 fuel blend at 1360 and 2000 rpm, as well as when using the B75 fuel blend at 1700 rpm. The lowest concentration of CO emissions for-

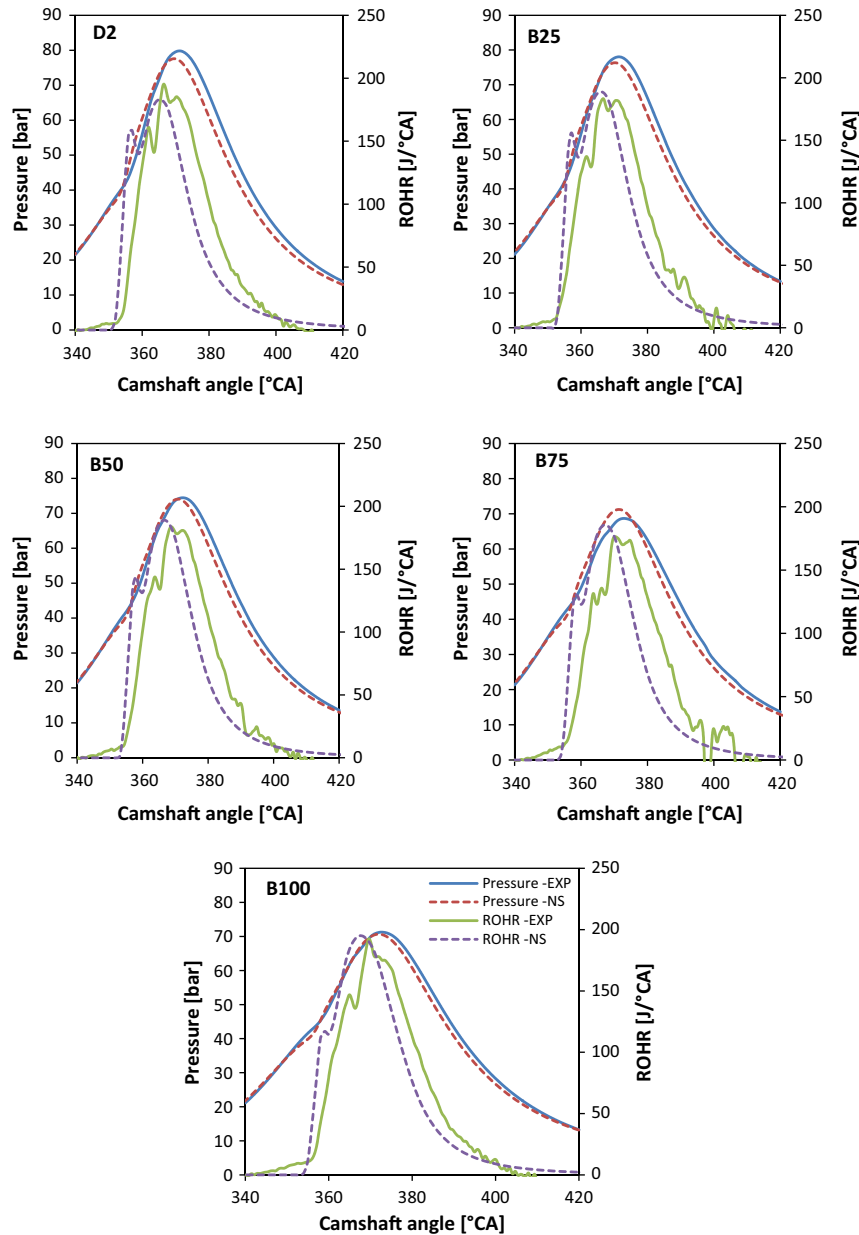


Fig. 8. Numerical and experimental results of in-cylinder pressure and rate of heat release at 1360 rpm.

matted was obtained numerically and experimentally when using pure biodiesel fuel on all engine speeds.

The numerical and experimental results of specific emissions agree well. The maximal difference between the numerical and experimental results was obtained using B25 fuel blend for NO_x and CO emissions. The average difference between the numerical and experimental results for the obtained specific emissions was 5%.

Fig. 7 shows the in-cylinder pressure curves for pure diesel fuel at 2000 rpm obtained using new and old sub-models for calculating combustion model parameters.

Simulation results, obtained with parameter values calculated using the new sub-model, have better agreement with the experimental results. The difference in the presented results between the new and old sub-models is the most significant between 340° and 360° of the camshaft rotation angle. The presented results confirm that new sub-model resolve the disadvantage of old sub-model for determination of precise combustion model parameters values.

This also increases our confidence in the numerical results obtained.

Figs. 8–10 show the numerical and experimental results of the in-cylinder pressure and rate of heat release (ROHR). The presented results indicate that when using biodiesel fuel the maximal value of in-cylinder pressure is decreased. The decrease of maximal in-cylinder pressure values is a result of lower biodiesel fuel calorific value and a retarded static fuel delivery angle. The numerical values for in-cylinder pressure are lower than the experimental value, except for the B75 fuel blend, where the opposite trend can be observed. The obtained curves of ROHR are typical for diesel engines using M-combustion systems, where diffusion combustion dominates. At low engine speed transitions from kinetic to diffusion combustion are noticeable. It clearly shows that the contribution of the kinetic part of combustion to the total amount of heat released is rather small. Increasing engine speed further decreases the contribution of the kinetic combustion phase to the total amount of heat released. This small contribution of kinetic part

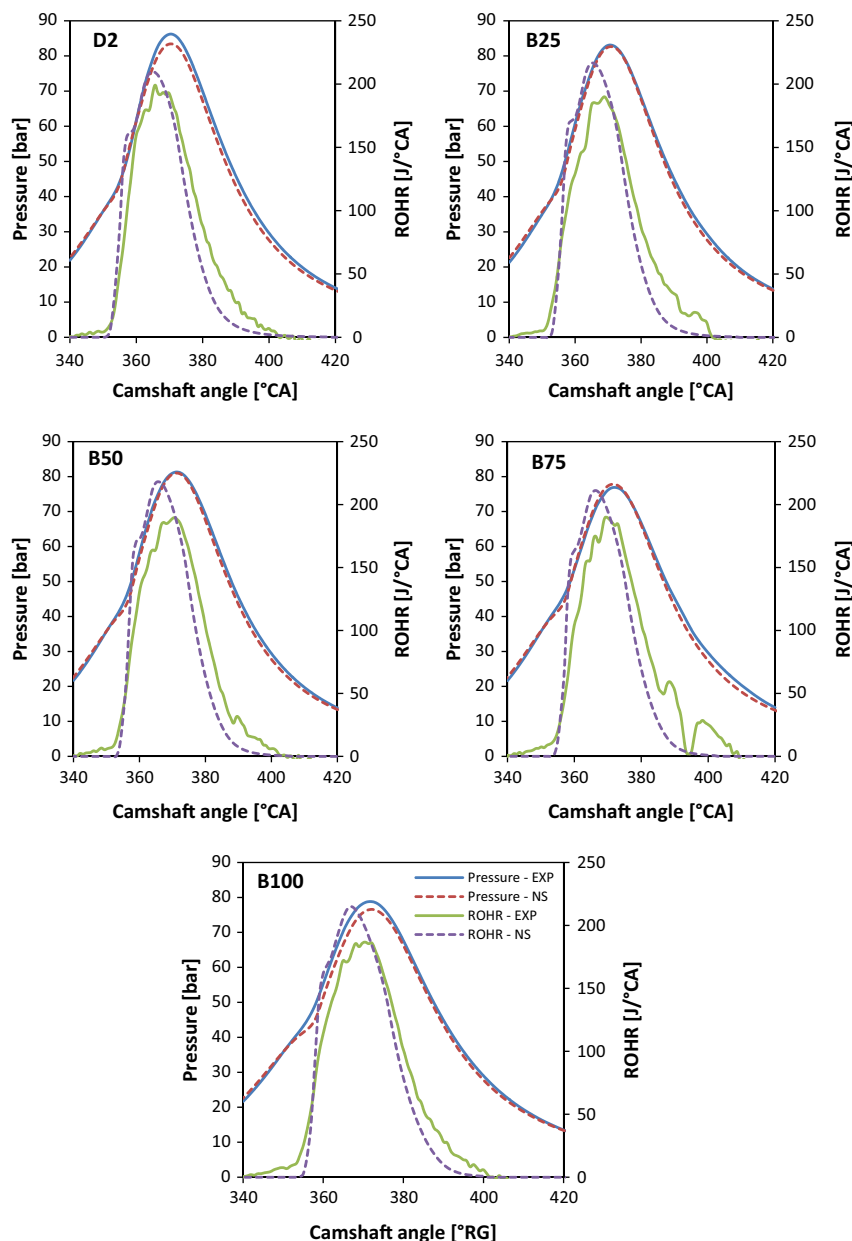


Fig. 9. Numerical and experimental results of in-cylinder pressure and rate of heat release at 1700 rpm.

of combustion is common for engines with M-combustion systems where the majority of fuel is injected onto the combustion chamber wall. The results of ROHR also indicate that when using biodiesel fuel or its blends the start of combustion is retarded.

The agreement between the numerical and experimental results for in-cylinder pressure is good and is within the range of pressure transducer measuring accuracy. The numerical and experimental curves of the rate of heat release have the same trends of

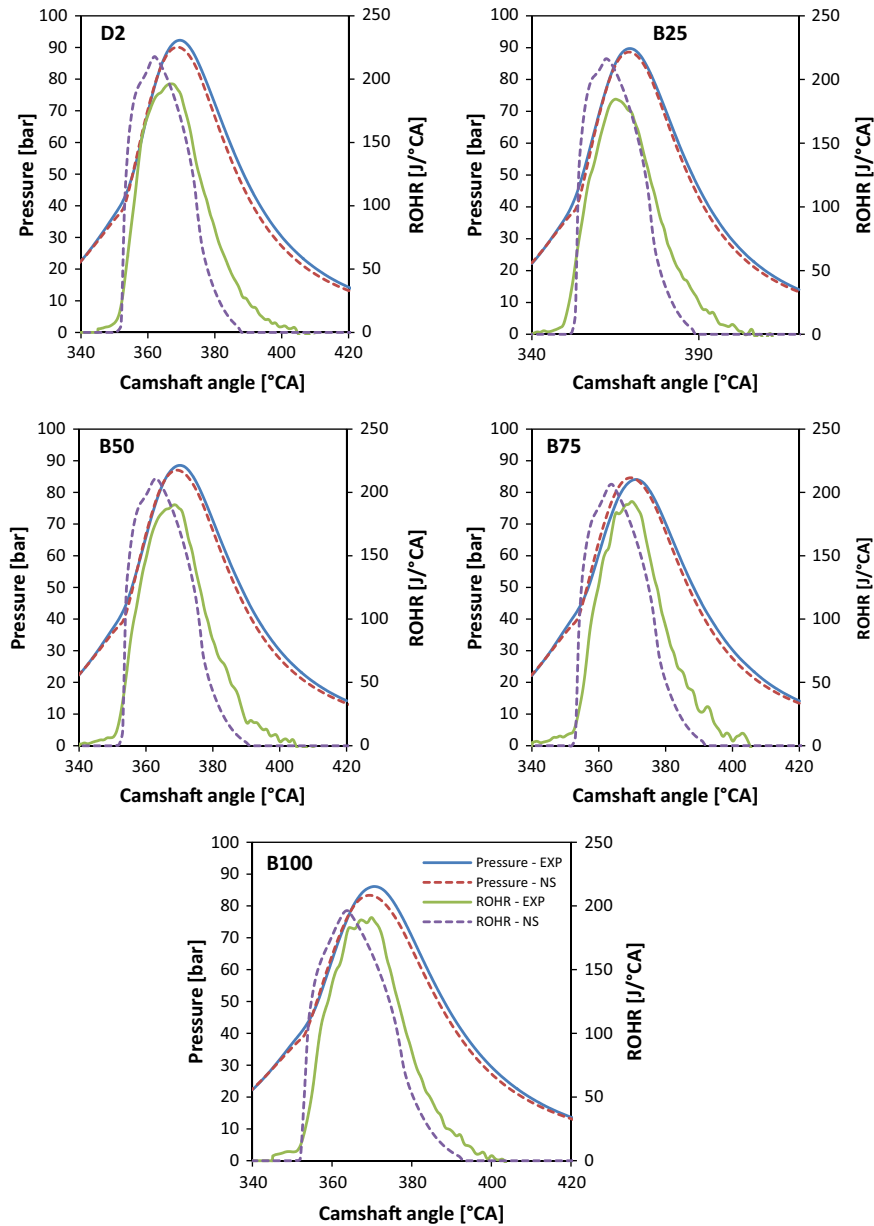


Fig. 10. Numerical and experimental results of in-cylinder pressure and rate of heat release at 2000 rpm.

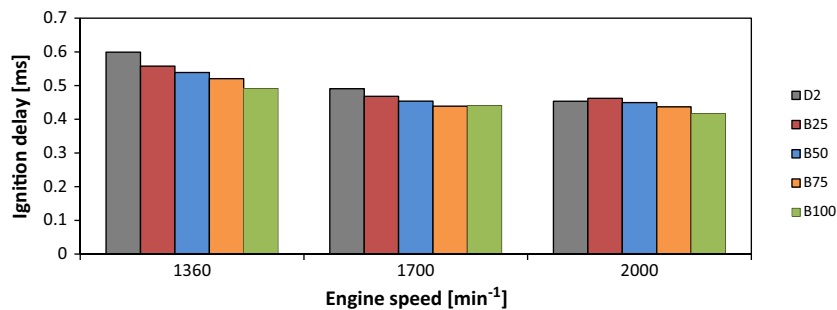


Fig. 11. Numerical results of ignition delay.

premixed and diffusion combustion phases. The difference between the numerical and experimental curves of ROHR can be attributed to the difference in models used for their calculation and is in the same range as in comparable studies, [20,21].

The tested fuel properties, static fuel delivery angle, and engine speed influence the duration of the ignition delay interval. The numerically-obtained results of ignition delay duration are presented in Fig. 11.

The numerical results of ignition delay indicate that increasing the percentage of biodiesel fuel decreases the duration of ignition delay. The highest decrease in ignition delay duration was obtained

at the lowest engine speed. The decrease in ignition delay duration is caused by the higher oxygen content and higher cetane number of the biodiesel fuel.

The numerical results of the accumulated NO_x emissions (NO_x accum.), accumulated CO emissions (CO accum.), and in-cylinder temperature are presented in Figs. 12–14.

The obtained numerical results for in-cylinder temperature on each test regime indicate that the maximal values of in-cylinder temperatures are decreased when using biodiesel fuel within a heavy-duty diesel engine. Lower in-cylinder temperatures are caused by lower caloric value and lower in-cylinder pressure of

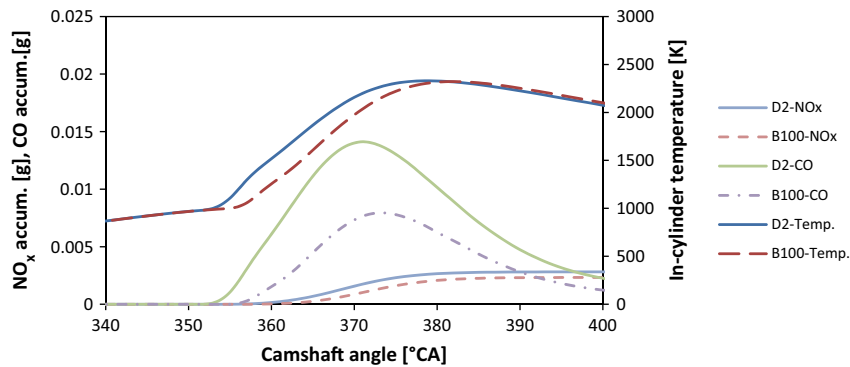


Fig. 12. Numerical results of emission formation and in-cylinder temperature at 1360 rpm.

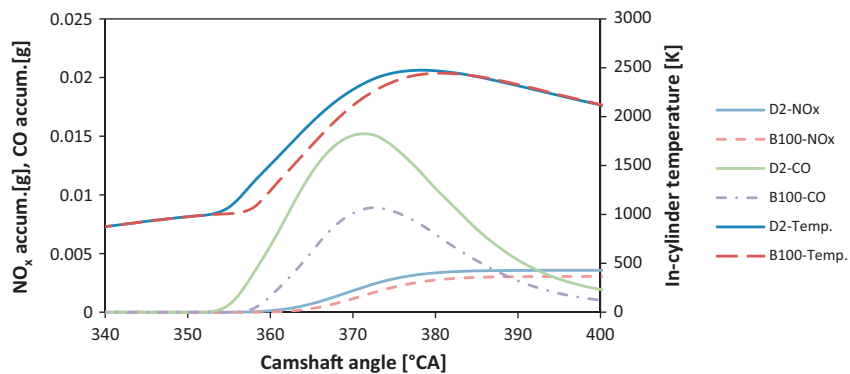


Fig. 13. Numerical results of emission formation and in-cylinder temperature at 1700 rpm.

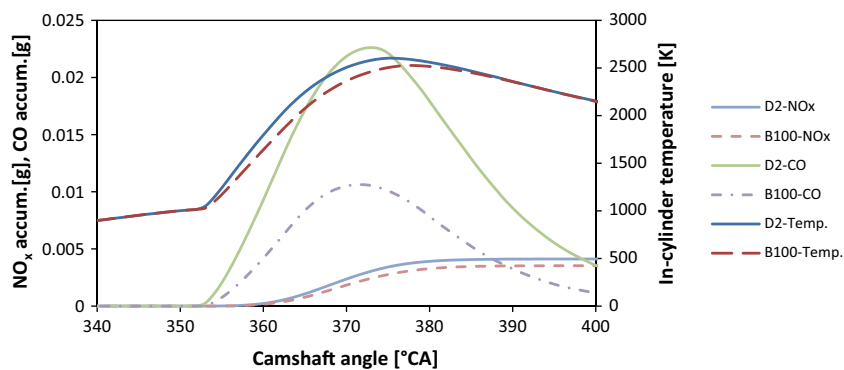


Fig. 14. Numerical results of emission formation and in-cylinder temperature at 2000 rpm.

biodiesel fuel and fuel blends. In general, an increase in engine speed results in a higher maximal in-cylinder temperature, which increases the thermal and total NO_x formation rates, Figs. 5 and 6.

The presented results also indicate that the start of temperature rise (start of combustion) is retarded when using biodiesel fuel. Lower values of in-cylinder temperature have an influence on the later start of NO_x and CO emission formation. It also results in a decrease of thermal NO_x emission formation, which are the largest contributors to the total amount of NO_x emissions. From the presented results of accumulated emissions it can be concluded that lower temperature decrease the NO_x formation rate. The temperature drop around 380 °CA freezes the formation of NO_x emissions. The decrease in formation rate can also be seen for the results of CO emissions. It can be concluded from accumulated amount of CO emissions that CO formation rates of biodiesel are much lower compared to diesel fuel. This can be attributed to difference in biodiesel chemical composition, which contains less carbon compared to diesel fuel, Table 1. The final total amount of CO emissions formatted is decreased because of the chemical reaction between CO and O₂ molecules which are taking place in expansion stroke.

7. Conclusions

The present paper studied the influence of mineral diesel fuel, pure biodiesel fuel and three blends of diesel and biodiesel fuel on diesel engine performance, combustion, and emission formation characteristics. Testing was performed numerically using the AVL BOOST simulation program, and experimentally using a test engine placed on an engine test-bed. The following conclusion can be made from the presented results:

- (1) The lower calorific value of biodiesel fuel and its blends influence the reduction of engine-rated torque on some test regimes compared to diesel fuel.
- (2) Higher density of biodiesel fuel increases the amount of injected fuel. This further influences the increase of brake-specific fuel consumption when increasing the percentage of biodiesel fuel in the fuel blend.
- (3) The different fuel composition of biodiesel influences the reduction of NO_x and CO emission when the percentage of biodiesel fuel is higher than 25%.
- (4) The use of biodiesel fuel reduces in-cylinder temperature, pressure, and heat release rate, which reduces thermal NO_x emission formation.
- (5) Higher oxygen content and a higher cetane number of biodiesel fuel reduce the duration of the numerical obtained ignition delay interval. It also contributes to a better oxidation process within the combustion chamber, which reduces the CO emission formation rate.
- (6) In general the numerical and experimental results agree well. The good agreement between the numerical and experimental results indicate that the proposed sub-models for determining combustion and emission model parameters are able to accurately determine the necessary parameter values if the fuel's properties and engine operating regimes are known. We can conclude that the proposed sub-model equations are suitable for calculation of needed combustion and emission models parameters for all fuels used in the presented paper.
- (7) The usage of the proposed sub-models reduces the time needed for the numerical testing of possible biodiesel fuel usage within heavy-duty diesel engines. It also enables us to run numerical simulations with a reasonable amount of confidence without experimental results. An improvement of the sub-model for determination of combustion model

parameters can be seen when comparing new simulation results of in-cylinder pressure to the results presented in previous work [23] in Fig. 7.

- (8) The proposed sub-models derivation is based on the measurement results for one test engine. In order to make them more widely used, several different measurements performed on different engines should be included in the sub-models' development. In this form, the proposed sub-models can be used with reasonable confidence for determining necessary model parameters for engines that are similar to our test engine.

Acknowledgement

This work was supported by AVL LIST GmbH, which provided the AVL-AST software and support during the research.

References

- [1] Markovič-Hribernik T, Murks Bašič A. Slovenia's climate policy efforts: CO₂ tax and implementation of EU ETS. *Climate Policy* 2007;7(2):139–55 [str.].
- [2] Demirbas A. Progress and recent trends in biodiesel fuels. *Energy Convers Manage* 2009;50.
- [3] Bahadur Magay S, Pelkonen P, Tahvanainen L, Toivonen R, Toppinen A. Growing trade of bioenergy in the EU: public acceptability, policy harmonization, European standards and certification needs. *Biomass Bioenergy* 2011;35:3318–27.
- [4] Alvarez R, Zubezu S, Diaz G, Lopez A. Analysis of low carbon super credit policy efficiency in European Union greenhouse gas emissions. *Energy* 2015;82:996–1010.
- [5] Torres Jiménez E, Svoltjšak M, Gregorc A, Lisec I, Pilar Dorado M, Kegl B. Physical and chemical properties of ethanol-biodiesel blends for diesel engines. *Energy Fuels* 2010;24(3):2002–9. <http://dx.doi.org/10.1021/ef901158a> [str.].
- [6] Azad AK, Rasul MG, Khan MMK, Sharma SC, Hazrat MA. Prospect of biofuels as an alternative transport fuel in Australia. *Renew Sustain Energy Rev* 2015;43:331–51.
- [7] Hribernik A, Kegl B. The influence of biodiesel fuel on the combustion and emission characteristics of a diesel engine. *J Mech Eng* 2007;53(10):683–95.
- [8] Bergthorson JM, Thomson MJ. A review of the combustion and emissions properties of advanced transportation biofuels and their impact on existing and future engines. *Renew Sustain Energy Rev* 2015;42:1393–417.
- [9] Lakshminarayanan PA, Aghav YV. Modelling diesel combustion, mechanical engineering series. Springer Science + Business Media B.V.; 2010. http://dx.doi.org/10.1007/978-90-481-3885-5_2.
- [10] Torres Jiménez E, Kegl M, Dorado R, Kegl B. Numerical injection characteristics analysis of various renewable fuel blends. *Fuel* 2012;97:832–42.
- [11] Kegl B. Effects of biodiesel on emissions of a bus diesel engine. *Bioresour Technol* 2008;99:863–73.
- [12] Hribernik A, Kegl B. Influence of biodiesel fuel on the combustion and emission formation in a direct injection (DI) Diesel engine. *Energy Fuels* 2007;21:1760–7.
- [13] Qi DH, Lee CF, Jia CC, Wang PP, Wu ST. Experimental investigation of combustion and emission characteristics of rapeseed oil–diesel blends in a two cylinder agricultural diesel engine. *Energy Convers Manage* 2014;77:227–32.
- [14] Can Ö. Combustion characteristics, performance and exhaust emissions of a diesel engine fueled with a waste cooking oil biodiesel blend. *Energy Convers Manage* 2014;87:676–86.
- [15] Arbab MI, Varman M, Masjuki HH, Kalam MA, Imtenan S, Sajjad H, et al. Evaluation of combustion, performance, and emission of optimum palm-coconut blend in turbocharged and non-turbocharged conditions of a diesel engine. *Energy Convers Manage* 2015;90:111–20.
- [16] How HG, Masjuki HH, Kalam MA, Teoh YH. An investigation of the engine performance, emissions and combustion characteristics of coconut biodiesel in a high-pressure common-rail engine. *Energy* 2014;69:749–59.
- [17] Awad S, Loubar K, Tazerout M. Experimental investigation on the combustion performance and pollutant emissions of biodiesel from animal fat residues on a direct injection diesel engine. *Energy* 2014;69:826–36.
- [18] Di Y, Cheung CS, Huang Z. Experimental study on particulate emission of a diesel engine fueled with blended ethanol–dodecanol–diesel. *Aerosol Sci* 2009;40:101–12.
- [19] Tse H, Leung CW, Cheung CS. Investigation on the combustion characteristics and particulate emission from a diesel engine fueled with diesel–biodiesel–ethanol blends. *Energy* 2015;83:343–50.
- [20] Zhou DZ, Yang WM, An H, Li J, Shu C. A numerical study on RRCl engine fueled by biodiesel/methanol. *Energy Convers Manage* 2015;89:798–807.
- [21] An H, Yang WM, Li J. Numerical modeling on a diesel engine fueled by biodiesel–methanol blends. *Energy Convers Manage* 2015;93:100–8.

- [22] Lešnik L, Vajda B, Žunič Z, Škerget L, Kegl B. The influence of biodiesel fuel on injection characteristics, diesel engine performance, and emission formation. *Appl Energy* 2013;111:558–70.
- [23] Lešnik L, Iljaž J, Hribernik A, Kegl B. Numerical and experimental study of combustion, performance and emission characteristic of a heavy-duty Di diesel engine running on diesel, biodiesel and their blends. *Energy Convers Manage* 2014;81:534–46.
- [24] Dobovišek Ž, Černej A, Hribernik A. Predictive zero-dimensional single-zone Diesel combustion simulation models. *J Mech Eng* 1993;39:137–60.
- [25] AVL List GmbH, AVL BOOST Theory, AVL List GmbH, Graz, v2012 edition; 2010.
- [26] Chmela F, Orthaber G. Rate of heat release prediction for direct injection diesel engines based on purely mixing controlled combustion. SAE Technical Paper 1999-01-0186.
- [27] Pattas K, Häfner G. Stickoxidbildung bei der ottomotorischen Verbrennung. *MTZ* 1973;12:397–404.
- [28] Onorati A, Ferrari G, D'Errico G. 1D unsteady flows with chemical reactions in the exhaust duct-system of S.I. engines: predictions and experiments. SAE Technical Paper 2001-01-0939.
- [29] Lešnik L, Kegl B. Usage of optimization methods for determination of combustion model parameters. In: V: international conference on innovative technologies IN-TECH 2013. Budapest, Hungary; 2013. p. 340–3.
- [30] Lešnik L, Vajda B, Zunič Z, Kegl B. Numerical and experimental research of spray characteristics. In: V: international conference on innovative technologies, IN-TECH 2011. Bratislava, Slovakia; 2011. p. 340–3 [str.].